Carboxyl Terminus of *Helicobacter pylori* α1,3-Fucosyltransferase Determines the Structure and Stability†

Sheng-Wei Lin,‡,§ Tsui-Min Yuan,‡,§ Jei-Ru Li,‡ and Chun-Hung Lin*,‡,§

Institute of Biological Chemistry and Genomics Research Center, Academia Sinica, No. 128 Academia Road Section 2, Nan-Kang, Taipei 11529, Taiwan, and Institute of Biochemical Sciences, College of Life Science, National Taiwan University, Taipei 10617, Taiwan

Received January 20, 2006; Revised Manuscript Received April 18, 2006

ABSTRACT: *Helicobacter pylori* is well known as the primary cause of gastritis, duodenal ulcers, and gastric cancer. The pathogenic bacteria produces Lewis x and Lewis y epitopes in the *O*-antigens of lipopolysaccharides to mimic the carbohydrate antigens of gastric epithelial cells to avoid detection by the host's immune system. The enzyme α1,3-fucosyltransferase from *H. pylori* catalyzes the glycosyl addition of fucose from the donor GDP-fucose to the acceptor *N*-acetyllactosamine. The poor solubility of the enzyme was resolved by systematic deletion of the *C*-terminus. We report here the first structural analysis using CD spectroscopy and analytical ultracentrifugation. The results indicate that up to 80 residues, including the tail rich in hydrophobic and positively charged residues (sequence 434−478) and 5 of the 10 tandem repeats of 7 amino acids each (399−433), can be removed without significant change in structure and catalysis. Half of the heptad repeats are required to maintain both the secondary and native quaternary structures. Removal of more residues in the *C*-terminus led to major structural alteration, which was correlated with the loss of enzymatic activity. In accordance with the thermal denaturation studies, the results support the idea that a higher number of tandem repeats functioning to facilitate a dimeric structure helps to prevent the protein from unfolding during incubation at higher temperatures.

Helicobacter pylori is a Gram-negative bacterium infecting about 50% of the human population worldwide. A major cause of chronic gastritis, duodenal ulcers (*1*, *2*), gastric adenocarcinoma, and mucosa-associated lymphoid tissue (MALT) lymphoma (*3*, *4*), this pathogen expresses adhesin proteins, such as BabA (*5*, *6*) and SabA (*7*, *8*), for attachment to specific glycoconjugates present on the gastric epithelial cell surface. The lipopolysaccharides (LPS)[1] of most *H. pylori* strains contain type 2 Lewis x, Lewis y and sialyl Lewis x structures in the antigenic *O*-polysaccharide chains, in addition to other minor variations. These structural epitopes are also found in mammalian tumor-associated carbohydrate antigens (*9*, *10*). Although the correlation of these Lewis antigens with *H. pylori* infection remains unclear (*11*), these glycoconjugates produced by *H. pylori* have been suggested to mimic host cell surface antigens, thus masking the pathogen from host immune surveillance (*12*). As a consequence, the generation of such antigens likely contributes to colonization and long-term *H. pylori* infection in the stomach (*13*, *14*). In addition, phase variation alters the expression of Lewis antigens, leading to the presence of several LPS variants in one bacterial cell population and the display of structural heterogeneity. This changing presentation of cell surface antigens represents a survival advantage for the bacteria (*15*, *16*).

Fucosyltransferases (FTs), which catalyze the transfer of fucose from GDP-fucose to various sugar acceptors, are the enzymes responsible for the last steps of A, B, H, and Lewis-related antigen biosynthesis. In *H. pylori*, the synthesis of Lewis b or y antigens requires α1,3/1,4-fucosylation prior to α1,2-fucosylation, unlike in mammalian cells where the latter reaction is followed by subterminal α1,3/1,4-fucosylation (*15*). The existence of FTs has been reported in vertebrates, invertebrates, plants, insects, parasites, and bacteria. All mammalian α1,3/4-FTs cloned so far have the typical domain structure of type II transmembrane proteins, consisting of a short *N*-terminal cytoplasmic tail, a transmembrane domain, and a stem region followed by a large *C*-terminal catalytic domain (*18*). The prokaryotic counterparts do not have the *N*-terminal tail and transmembrane domain. In contrast to mammalian enzymes, *H. pylori* has a catalytic domain located at the *N*-terminus. The *C*-terminal sequence of *H. pylori* FTs has 2−10 repeats of 7 amino acids (known as heptad repeats), followed by a highly conserved region rich in basic and hydrophobic residues (*19*, *20*). The heptad repeats are proposed to form a leucine zipper as the determinant for a dimeric structure. The region containing basic and hydrophobic residues is qualified for the formation of amphipathic helices, suggesting that the *H. pylori* protein is membrane-associated (*18*). *H. pylori* and mammalian α1,3/4-FTs are highly divergent in overall amino acid sequence, possibly reflecting the differences in substrate specificity and functional roles in biosynthesis. This sequence divergence

† This work was supported by the National Science Council (NSC-94-2113-M-001-028) and Academia Sinica, Taiwan.

* Corresponding author. Phone: +886-2-27890110. Fax: + 886-2-26514705. E-mail: chunhung@gate.sinica.edu.tw.

‡ Academia Sinica.

§ National Taiwan University.

[1] Abbreviations: LPS, lipopolysaccharides; FT, fucosyltransferase; LacNAc, *N*-acetyllactosamine; CD, Circular dichroism.

10.1021/bi0601297 CCC: $33.50 © 2006 American Chemical Society
Published on Web 06/08/2006

Table 1: Primer Sequences Used in PCR Experiments to Construct the Desired Plasmids

FTΔ0F	5′-GGG AAT TCC ATA TGT TCC AAC CCC TAT TAG AC-3
FTΔ0R	5′-CCC CCA CTC GAG CCA ACC CAA TTT TTT AAC-3′
FTΔ9R	5′-CCC ACT CGA GTA TGG CGC GCA ACA AAG G-3
FTΔ23R	5′-GGT AAG CCT CGA GAT AGA TTT TAG AAG TGG TG-3′
FTΔ28R	5′-GAT TTT CTC GAG GGT GTT TTG GGA TAA TTC-3′
FTΔ38R	5′-TCT TTT TTC TCG AGA GCT TTT GAT AA-3′
FTΔ45R	5′-GAG CTC GAG ATA ATT AAC CCT CAA ATC-3′
FTΔ66R	5′-ATT AAC CCT CAA CTC GAG ATA ATT AAT TCT CAA ATC-3
FTΔ80R	5′-ATT AAC CCT CAA CTC GAG ATA ATT AAT TCT CAA ATC-3
FTΔ110R	5′-CAA ATC ATC CTC GAG AAC CCT CAA ATC ATC-3′
FTΔ115R	5′-CCT CAA CTC GAG AAT AGT TAC TAA AGG CTC-3′

makes the *H. pylori* enzyme an attractive target for therapeutic intervention.

Previously, our preliminary result demonstrated that the systematic deletion of the *C*-terminus of the α1,3-FT from *H. pylori* NCTC11639 greatly improves the marginal solubility of the full-length protein (*21*). The *C*-terminal residues previously studied include 10 tandem repeats (corresponding to the sequence 364−433) and a region rich in positive and hydrophobic residues (sequence 434−478). In this report, we characterized these truncated forms and demonstrated that the number of heptad repeats is correlated with both the stability of the secondary and quaternary structures as well as enzyme activity. Five or more heptad repeats help to maintain the structural integrity and full enzyme activity.

EXPERIMENTAL PROCEDURES

Materials. Oligosaccharides, Galβ(1,4)GlcNAc, Galβ(1,3)-GlcNAc, NeuAcα(2,3)Galβ(1,4)GlcNAc, NeuAcα(2,6)Galβ-(1,4)GlcNAc, and GlcNAcβ(1,4)GlcNAc were obtained from Toronto Research Chemicals (North York, Canada). Galβ-(1,6)GlcNAc was purchased from Seikagaku Corp. (Tokyo, Japan). Pyruvate kinase type VII from rabbit muscle, L-lactic dehydrogenase type XXXIX from rabbit muscle, GDP-fucose, phosphoenol pyruvic acid (PEP), β-NADH, and Fucα(1,2)Galβ(1,4)GlcNAc were obtained from Sigma (St. Louis, MO). The HiTrap chelating high performance (HP) column was from Amersham Biosciences (Uppsala, Sweden). All restriction enzymes were purchased from New England Biolabs (Ipswich, MA). All other chemicals of reagent grade were purchased from Merck, Difco, and Life Technologies.

DNA Manipulation and Cloning of Chimeric FTs. Standard DNA manipulation techniques, including the isolation, transformation, and restriction enzyme digestion analysis of plasmid DNA, were followed according to Sambrook et al. (*22*). The FT gene was cloned from *H. pylori* (NCTC 11639) genomic DNA. According to the reported sequence (GenBank accession no. af008596), the plasmid was constructed to produce α1,3-FT with a hexahistidine tag at the *C*-terminus using the sense primer FTΔ0F with an *Nde*I restriction site and the antisense primer FTΔ0R with an *Xho*I restriction site. Analogously, the plasmids of various truncated forms (FTΔ9, FTΔ23, FTΔ28, FTΔ38, FTΔ45, FTΔ66, FTΔ80, FTΔ110, and FTΔ115) were constructed using the same sense primer FTΔ0F and different antisense primers (see Table 1 for details). The usage of the restriction sites of *Nde*I and *Xho*I allowed cloning into a similarly digested pET-21b. The coding region of these FT genes was controlled by the T7 promoter. The ligated plasmids were transformed into *E. coli* DH5α or *E. coli* BL21 (DE3) for expression. The cloned genes were sequenced to ensure that no mutations occurred during their construction.

Protein Expression and Purification. For expression, the clones were cultured in LB broth containing 100 μg/mL of ampicillin with agitation at 37 °C until A_{600} reached 0.5. Expression was induced by the addition of 0.1 mM isopropyl-1-thio-β-D-galactopyranoside (IPTG) at 25 °C for 5 h, after which the culture was harvested by centrifugation and lysed by the following procedure. The cell pellets were resuspended in the lysis buffer (phosphate-buffered saline), disrupted by French press at 16 000 psi and centrifuged at 15 000*g* at 4 °C for 20 min. The supernatant was subjected to ultracentrifugation at 125 000*g* at 4 °C for 1 h to separate the soluble proteins from the inclusion bodies. The supernatant was applied to a HiTrap chelating HP column according to the instruction manual. The desired fractions were pooled and dialyzed in 50 mM Tris buffer (pH 8.0) to yield the protein with more than 98% homogeneity. The protein concentration was determined using the Bio-Rad Protein Assay kit based on the Bradford method, with bovine serum albumin as a standard.

Immunoblot Analysis of Chimeric FT Expression. Crude cell extracts and supernatants were boiled for 5 min in 2% SDS, 0.1% bromophenol blue, and 10% 2-mercaptoethanol. The samples were separated by 10% SDS−PAGE, and the proteins were electrically transferred to PVDF. The blots were probed with primary antibody (mouse anti-His_6 monoclonal antibody) at 1:5000 dilution and secondary antibody (alkaline phosphatase-conjugated goat anti-mouse IgG) at 1:7500 dilution.

Fluorometric Assay for FT Activity. FTs produce GDP as the side product. This reaction was coupled with the pyruvate kinase/lactate dehydrogenase assay to monitor the consumption of NADH (*23*) with an excitation at 340 nm and emission at 460 nm as a means of measuring FT actitivity. The activity was measured at 25 °C for 5 min in a final volume of 0.4 mL containing 100 mM Tris (pH 7.5), 1 mM $MnCl_2$, 1 mM PEP, 50 μM NADH, 13.5 U pyruvate kinase, 30 U lactate dehydrogenase, 4 mM *N*-acetyllactosamine (LacNAc), and 400 μM GDP-fucose. The assay was initiated upon the addition of purified FT, and the decrease in the fluorescence emission at 460 nm was monitored. One unit of enzyme activity is defined as the consumption of 1 μmol of GDP-fucose or the formation of an equal amount of Lewis x (reaction product) per minute.

Kinetics Analysis and Acceptor Specificity Study. Kinetic parameters were measured for the acceptor substrate LacNAc and the donor GDP-fucose. In the former, the reaction rates were measured with 0−50 mM LacNAc and 400 μM GDP-fucose, whereas 0−1.5 mM GDP-fucose and 4 mM LacNAc

were applied for the latter. The resulting data were transferred to the software KaleidaGraph and fitted by the Michaelis−Menten equation. For the substrate specificity study, 1 mM sugar substrates were used to measure the relative rates.

Circular Dichroism Analysis. Circular dichroism (CD) spectrometry was performed using a JascoJ-715 spectropolarimeter under constant N_2 flush. The wavelength scan data was recorded using 0.1-cm path length quartz cuvettes. The far UV CD spectra were measured at 190−250 nm with a 2.0 bandwidth and a 0.1 nm resolution at a scan speed of 20 nm/min. Ten repetitive scans were averaged. All CD spectra were corrected for their respective buffer blanks**.** The CD spectra were obtained at 25 °C, and the protein concentrations were 0.03−0.3 mg/mL in 50 mM Tris buffer (pH 8.0). The mean residue ellipticity ([θ]) at each wavelength was calculated from the equation, $[\theta] = MRW \cdot \theta_\lambda / 10 \cdot d \cdot c$. *MRW* is the mean residue weight, θ_λ is the measured ellipticity in degrees at wavelength λ, d is the cuvette path length (0.1 cm), and c is the protein concentration in mg/mL. The deconvolution was performed using online CD analysis by DICHROWEB, which is available via the Internet at http://www.cryst.bbk.ac.uk/cdweb/html/home.html and offers several important pieces of analysis software for secondary structure determination, such as CONTINL, SELCON3, CDSSTR, and K2D.

Analytical Ultracentrifugation. Sedimentation coefficients and molar masses were analyzed by analytical ultracentrifugation. Prior to the experiments, protein samples in 50 mM Tris buffer (pH 8.0) were diluted to 0.03−0.30 mg/mL. Sedimentation velocity studies were carried out with a Beckman Optima XL-A analytical ultracentrifuge with an An60Ti rotor at 20 °C and 40 000 rpm. Protein samples loaded onto standard double sector cells with aluminum or Epon charcoal-filled centerpieces. The UV absorption of the cells was scanned at 280 nm (for the concentration of 0.3 mg/mL) or 230 nm (for the concentration of 0.03 mg/mL) in a continuous mode, every 10 min for a period of 5 h. The data were analyzed with Sedfit version 8.9d program. Collections of 10−15 radical scans were used for analysis, and 200 sedimentation coefficients between 2 and 10 *S* were employed in calculating the $c(S)$ distribution. The positions of the meniscus and cell bottom were determined by visual inspection and then refined in the final fit. The partial specific volumes for FTΔ28, FTΔ45, FTΔ66, FTΔ80, and FTΔ115 were calculated from the amino acid compositions to be 0.7291, 0.7283, 0.7302, 0.7309, 0.7322 mL/g, respectively. The solvent density and viscosity were calculated with the program Sednterp version 1.08. All of the samples were visually checked for clarity after ultracentrifugation, and no indication of precipitation was found. After protein samples were loaded on six-hole charcoal-filled Epon centerpieces, equilibrium sedimentation centrifugations were carried out at 14 000, 18 000, and 20 000 rpm at 4 °C until equilibrium was reached. The equilibrium scans were analyzed by the software provided by Beckman-Coulter with a self-association mode. The data were analyzed for average molecular mass in terms of a single homogeneous species.

Thermal Denaturation. Various truncated enzymes of 0.30 mg/mL in 50 mM Tris (pH 8.0) were heat-treated for temperature-dependent denaturation and aggregation. The studies were measured by detecting the optical density of light-scattering aggregates at 340 nm with a Perkin-Elmer Lambda Bio 40 UV/VIS spectrophotometer. The heating rate was 1 °C/min. Time-dependent aggregation was measured at 55 °C at 340 nm. Additionally, CD melting curves were determined by monitoring the changes in the dichroic intensity at 222 nm as a function of temperature. Protein samples were 0.03−0.3 mg/mL in Tris buffer (pH 8.0). Thermal denaturation was studied in the range from 25 to 90 °C with 1 °C increments. The denaturation process was characterized by determining the midpoint of denaturation (T_d). T_d is the temperature at which half of the protein is in a denatured state and the other half is in a native state.

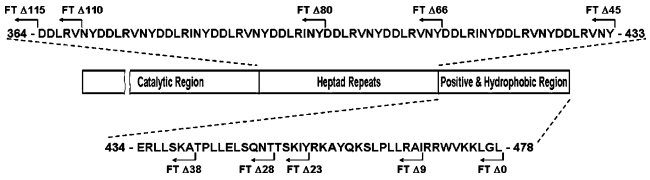

FIGURE 1: Full-length and truncation mutants of α1,3-FT. The deletion studies focused on the *C*-terminal 115 residues, including the heptad repeats and the region of positive and hydrophobic residues (the protein domains are not represented according to their relative size). The mutants missing the *C*-terminal 9, 23, 28, 38, 45, 66, 80, 110, and 115 residues are designated as FTΔ9, FTΔ23, FTΔ28, FTΔ38, FTΔ45, FTΔ66, FTΔ80, FTΔ110, and FTΔ115, respectively. FTΔ0 represents the full-length enzyme.

RESULTS

Preparation of Chimeric FTs. Recombinant *H. pylori* FT was insoluble in our hands despite attempting various isolation approaches, including a trial of detergents to solublize the protein as well as the alteration of induction temperature and/or IPTG concentration. A number of expression vectors that have been successfully used to coexpress fusion proteins were also tested as expression vectors for FT, such as pET-43a containing nus, pTYB11 containing a chitin binding domain, pET-42a containing glutathione-*S*-transferase, pET-32a containing thioredoxin, pCAL containing calmodulin binding protein, and pMAL containing maltose binding protein. These procedures all failed to generate an acceptable protein yield because of poor expression, protein insolubility, or the occurrence of degradation. As mentioned above, the *C*-terminal 115 residues are not expected to be directly involved in the enzyme reaction mechanism. Thus, these residues were deleted in an attempt to improve solubility. Nine different truncated forms with *C*-terminal deletions of 9, 23, 28, 38, 45, 66, 80, 110, and 115 residues were prepared and designated as FTΔ9, FTΔ23, FTΔ28, FTΔ38, FTΔ45, FTΔ66, FTΔ80, FTΔ110, and FTΔ115, respectively (Figure 1). All of the proteins were prepared with a hexahistidine tag at the *C*-terminus under the same conditions and expressed at a level comparable to that of the full-length FT (FTΔ0), indicating that the truncation did not affect protein expression (Figure 2A). According to PAGE analysis followed by immunoblot detection, all of the variants except for FTΔ0 and FTΔ9 were obtained as soluble forms after ultracentrifugation at 100 000*g* (Figure 2B). Further purification by nickel affinity chromatography yielded about 1 mg of FTΔ23, 2−3 mg of FTΔ28 and FTΔ38, 15 mg of FTΔ45 and FTΔ66, and 20 mg of the three other smaller forms per liter culture. The deletion of the *C*-terminal 45 amino acids considerably improved the solubility of the protein. Thus, the putative membrane-

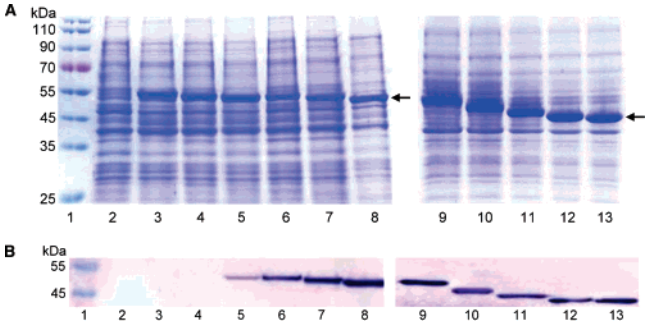

FIGURE 2: Protein expression and supernatant analysis of various chimeric FTs. (A) SDS−PAGE of the cultured cell lysate. Cultures of *E. coli* BL21(DE3) containing pET-21b or various chimeric FT plasmids were induced with 0.1 mM IPTG at 25 °C for 5 h, harvested by centrifugation, and then analyzed by Coomassie blue staining following electrophoresis on a 10% SDS-polyacrylamide gel. The arrows designate the bands of interest. (B) Immunoblot of soluble chimeric FTs. After cell disruption by French press and centrifugation, the supernatant was further subjected to ultracentrifugation, resolved on a 10% SDS-polyacrylamide gel, and transferred to a PVDF membrane. The FT proteins were detected with mouse anti-His_6 monoclonal antibody. Lane 1: molecular weight marker (sized indicated in kDa); lane 2: cell extract of the host strain with pET-21b alone; lanes 3−13: cell extracts from the recombinant cells of various FT clones, FTΔ0 (lane 3), FTΔ9 (lane 4), FTΔ23 (lane 5), FTΔ28 (lane 6), FTΔ38 (lane 7), FTΔ45 (lanes 8 and 9), FTΔ66 (lane 10), FTΔ80 (lane 11), FTΔ110 (lane 12), and FTΔ115 (lane 13).

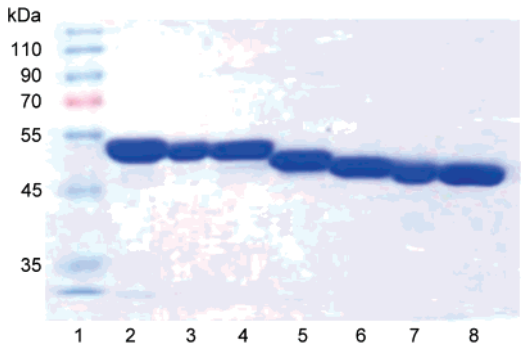

FIGURE 3: SDS−PAGE analysis of various purified FTs. Lane 1: molecular weight marker (sized indicated in kDa); lanes 2−8: FTΔ28 (lane 2), FTΔ38 (lane 3), FTΔ45 (lane 4), FTΔ66 (lane 5), FTΔ80 (lane 6), FTΔ110 (lane 7), and FTΔ115 (lane 8). All of the proteins were purified by a HiTrap chelating HP column (nickel affinity chromatography) after cell lysis and subsequent centrifugation.

associated region can be removed to greatly improve protein yield. These proteins were obtained at >95% homogeneity (Figure 3) and made it possible to carry out further investigations without use of radioisotope-labeled substrates, excluding FTΔ23, which had limited purity due to weak binding to the affinity column.

Biochemical Characterizations of Chimeric FTs. The FT activity was measured on the basis of a fluorometric method to monitor GDP production using a pyruvate kinase/lactate dehydrogenase-coupled enzymatic assay for the consumption of NADH (*23*). FTΔ0 and FTΔ9 were not studied because of their limited solubility. According to their kinetic parameters (Table 2), the five proteins FTΔ28, FTΔ38, FTΔ45, FTΔ66, and FTΔ80 had comparable activities, implying that at least 80 residues can be removed from the *C*-terminus without changing the activity. No apparent differences were found in K_m and V_{max} values for both acceptor (LacNAc) and donor (GDP-fucose) substrates as long as the *C*-terminal deletion was restricted to 80 residues. The specific activity (5.82 μmol/mg·min) was at least 2000-fold higher than the previously reported values, likely because of the high purity and increased solubility (*19*, *24*). However, the removal of additional residues led to a dramatic loss in activity, as shown by the several-fold increase in the K_m values and the decrease in the V_{max} values of FTΔ115 (FTΔ110 had an activity similar to that of FTΔ115; data not shown).

Furthermore, these truncated FTs are highly specific for the type 2 sugar substrates that contain the Galβ-1,4-GlcNAc structure, consistent with an earlier report regarding the full-length enzyme (*25*). FTΔ45 did not accept the type 1 substrate (Galβ-1,3-GlcNAc), as shown in Table 3. In addition to glycosidic linkage, the presence of both sugar units of LacNAc was essential to the specificity, as demonstrated by the comparison of LacNAc with GlcNAcβ-1,4-GlcNAc and Galβ-1,4-Glc (lactose). The FT could tolerate additional 1,2-fucosylation or 2,3-sialylation but not the 2,6-sialylation introduced to the galactose of LacNAc. The modification at the reducing end was allowed, as shown by the fact the enzyme accepts the introduction of a triazole group, in agreement with the reported acceptance of modified LacNAc with a long alkyl chain in the reducing terminus (*25*). Moreover, further truncation did not appear to change the specificity because the results for FTΔ80 and FTΔ115 were similar to those found for FTΔ45 (data not shown).

Structural Characterizations of Chimeric FTs. To understand why the *C*-terminal truncation of 115 residues rather than that of 80 or fewer residues is associated with activity loss, the secondary structures of FTΔ28, FTΔ45, FTΔ66, FTΔ80, and FTΔ115 were compared using far-UV CD spectroscopy. Figure 4 shows their CD spectra recorded from 190 to 250 nm. The mean residue ellipticity ([θ]) was computed from the original CD reading in accordance with the amino acid residue concentration and the path length. CD spectra were examined at different protein concentrations, and the results revealed no concentration dependence (data not shown). The spectra were further analyzed by the programs CONTIN, SELCON3, K2D, and CDSSTR, all of which produced consistent simulations (*26*−*28*). Table 4 shows the analysis of secondary structure according to the CDSSTR method. The CD spectra of *H. pylori* α1,3-FTs did not decrease in intensity following *C*-terminal deletion until all 115 residues were removed. The estimation of protein secondary structure fractions from CD spectra by the CDSSTR method indicated a relative loss of 13% of the α-helix with the concomitant gain of 10% of the β-strand upon the removal of 70 residues from FTΔ45 to FTΔ115 (Table 4). Although the tandem heptads and the hydrophobic and basic residues were suggested to form mainly α-helices, no obvious changes were found in the CD spectra of FTΔ28, FTΔ45, FTΔ66, and FTΔ80. In contrast, only FTΔ115, lacking the whole repeat region, exhibited substantial changes in the secondary structure.

In addition, the quaternary structure of these chimeric FTs was examined by analytical ultracentrifugation. A single species was detected for each protein (Figure 5) in sedimentation velocity studies, suggesting that they are structurally homogeneous in solution. Two different protein concentrations (0.03 and 0.3 mg/mL) were studied, and the results were found to be consistent. The experimental data represents

Table 2: Michaelis−Menten Parameters of Chimeric FTs[a]

FT (specific activity, U/mg)[b]	LacNAc K_m (mM)	LacNAc V_{max} (μmol/min·mg)	LacNAc V_{max}/K_m	GDP-fucose K_m (μM)	GDP-fucose V_{max} (μmol/min·mg)	GDP-fucose V_{max}/K_m
FTΔ23 (2.52)	0.78 ± 0.09	2.97 ± 0.08	3.81	68.30 ± 5.32	2.85 ± 0.06	0.042
FTΔ28 (4.84)	0.78 ± 0.05	4.39 ± 0.07	5.63	93.56 ± 3.82	6.58 ± 0.07	0.070
FTΔ38 (5.04)	0.70 ± 0.07	4.84 ± 0.10	6.91	79.67 ± 6.01	5.26 ± 0.12	0.066
FTΔ45 (5.72)	0.71 ± 0.06	5.28 ± 0.14	7.44	88.31 ± 8.68	5.32 ± 0.14	0.060
FTΔ66 (5.82)	0.71 ± 0.03	6.34 ± 0.09	8.57	78.64 ± 3.03	6.56 ± 0.06	0.083
FTΔ80 (5.20)	0.89 ± 0.09	6.40 ± 0.17	7.19	98.64 ± 5.34	6.27 ± 0.11	0.064
FTΔ115 (0.38)	8.92 ± 1.61	1.48 ± 0.08	0.17	222.8 ± 32.2	1.35 ± 0.06	0.006

[a] The enzyme activity was coupled with a pyruvate kinase/lactate dehydrogenase assay that measures NADH consumption by detecting the fluorescence emission at 460 nm. The reaction assay was initiated upon the addition of purified FT at 25 °C in a final volume of 0.4 mL containing 100 mM Tris buffer (pH 7.5), 1 mM $MnCl_2$, 1 mM PEP, 50 μM NADH, pyruvate kinase (13.5 U), 30 U lactate dehydrogenase, LacNAc, and GDP-fucose. Various concentrations (0−50 mM) of LacNAc and 400 μM GDP-fucose were used to determine the K_m values of LacNAc. Likewise, 4 mM LacNAc and various concentrations (0−1.5 mM) of GDP-fucose were used to determine the K_m values of GDP-fucose. [b] One unit (U) = 1 μmol of product formation per minute.

Table 3. Acceptor Substrate Specificity of FTΔ45[a]

Structure of Galβ(1,4)GlcNAc-triazole

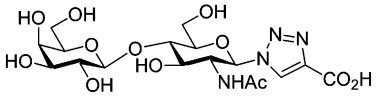

substrate (1 mM)	relative activity (%) FTΔ45
Galβ(1,4)GlcNAc	100
Fucα(1,2)Galβ(1,4)GlcNAc	138
Galβ(1,4)GlcNAc-triazole	49.6
GlcNAcβ(1,4)GlcNAc	3.30
NeuAcα(2,3)Galβ(1,4)GlcNAc	20.7
NeuAcα(2,6)Galβ(1,4)GlcNAc	<0.1
Galβ(1,3)GlcNAc	<0.1
Galβ(1,6)GlcNAc	<0.1
Galβ(1,4)Glc	0.60

[a] The activity was measured by the coupled enzyme assay at 25 °C for 5 min in a final volume of 0.4 mL containing 100 mM Tris buffer (pH 7.5), 1 mM $MnCl_2$, 1 mM PEP, 50 μM NADH, 13.5 U pyruvate kinase, 30 U lactate dehydrogenase, 1 mM acceptor substrate, and 400 μM of GDP-fucose. The numbers were normalized on the basis of the value of Galβ(1,4)GlcNAc.

the best-fit sedimentation profiles for the continuous size distribution analyzed by the Sedfit program (version 8.9d). The gray scale of the residual bitmap showed a high quality fit. The fitting results are shown as calculated: $c(S)$ versus the sedimentation coefficient (Figure 5A) or calculated $c(M)$ versus the mass (Figure 5B). The results indicated that FTΔ28, FTΔ45, FTΔ66, and FTΔ80 had very similar sedimentation patterns at ~5.3 S, whereas the S value of FTΔ115 was shifted to 3.5. On the basis of the results of the $c(M)$ distribution, the molecular masses of the chimeric FTs were estimated to be 105, 100, 97, 90, and 41 kDa for FTΔ28, FTΔ45 FTΔ66, FTΔ80, and FTΔ115, respectively. In accordance with the theoretical mass of each polypeptide, 53 766, 51 871, 49 229, 47 477 and 43 069 Da corresponding to FTΔ28, FTΔ45 FTΔ66, FTΔ80 and FTΔ115, respectively, the first four proteins exist as dimers in solution, whereas FTΔ115 is a monomer.

To corroborate the information on the quaternary structure of these truncated FTs, sedimentation equilibrium experiments were performed at 4 °C at three different ultracentrifugation speeds with a protein concentration of 0.3 mg/mL. Each data set, which was analyzed separately, gave a single homogeneous species. A simultaneous fit was then performed for FTΔ45 and FTΔ115 to yield an average mass of 115 671 and 45 967 Da, respectively (Figure 6). The result confirmed the molecular mass determination by the sedimentation velocity experiments. Taken together, the deletion of the *C*-terminal 115 residues had apparent alterations in both the secondary and quaternary native structure. In contrast, no perceivable change was observed with the removal of 80 or fewer residues, indicating that one-half of the heptad repeats can be deleted without affecting structural integrity.

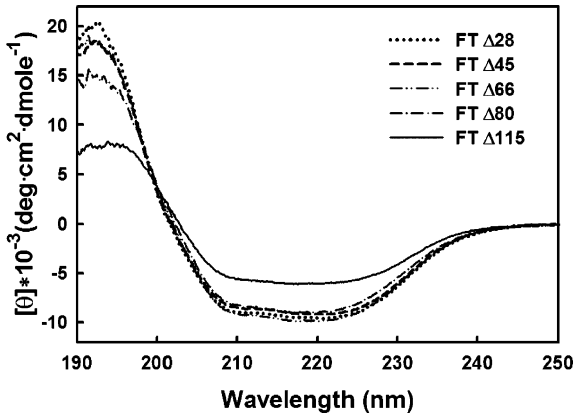

FIGURE 4: CD spectra of FTΔ28, FTΔ45, FTΔ66, FTΔ80, and FTΔ115 in the far-UV region. The CD spectra were obtained at 25 °C, and the protein concentrations were 0.03−0.30 mg/mL in 50 mM Tris buffer (pH 8.0) in a 0.1-cm light path CD cell. After background subtraction, the CD data were converted from CD signals into mean residue ellipticity values (degrees·cm^2·$dmol^{-1}$).

Table 4. Percent Secondary Structure Contents of Various FTs (FTΔ28, FTΔ45, FTΔ66, FTΔ80, and FTΔ115)[a]

	α-helix (%)	β-strand (%)	random coil (%)	rormalized rmsd
FTΔ28	31	21	47	0.016
FTΔ45	27	23	48	0.018
FTΔ66	28	22	49	0.016
FTΔ80	26	23	49	0.017
FTΔ115	14	33	53	0.033

[a] The results are derived from the analysis of the CD spectra (Figure 4) on the basis of the CDSSTR method.

Thermostability of Chimeric FTs. We found that the smaller truncated proteins, especially FTΔ115, tended to precipitate in solution during the studies. This observation

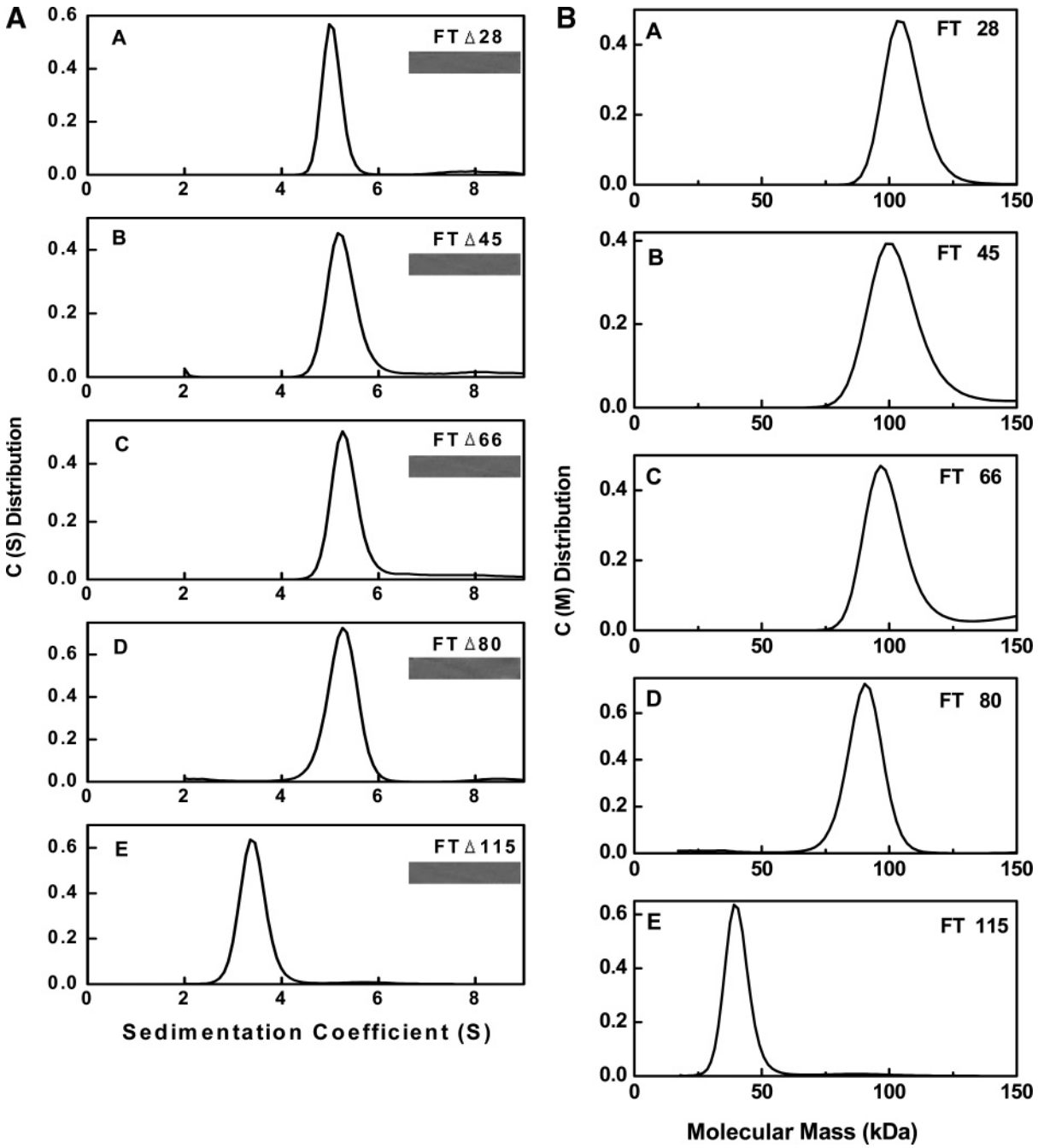

FIGURE 5: Sedimentation velocity studies of various truncated FTs. (A) Distribution of the sedimentation coefficients of FTΔ28, FTΔ45, FTΔ66, FTΔ80, and FTΔ115 in 50 mM Tris buffer (pH 8.0). (B) Distribution of the molecular masses of these proteins.

prompted us to investigate whether the *C*-terminus also plays a role in protein aggregation and/or stability. Proteins FTΔ28, FTΔ45, FTΔ66, FTΔ80, and FTΔ115 (0.3 mg/mL each) were analyzed for their ability to withstand irreversible thermal inactivation by monitoring the optical density at UV 340 nm due to the light scattering aggregates upon heating (30−85 °C), as shown in Figure 7A. Two of the largest chimeric proteins tested, FTΔ28 and FTΔ45, were stable and did not exhibit any turbidity during the heating process. The other proteins, FTΔ66, FTΔ80 and FTΔ115, aggregated to form precipitates during the heating process, and the derived temperatures for the onset of aggregation (T_{agg} values) were 78, 76, and 74 °C, respectively. The T_{agg} values were lower for smaller FT chimeras. A similar result was obtained in a time-dependent study in which all of the proteins were heated to 55 °C (Figure 7B). The delay times (t_d) of FTΔ66, FTΔ80, and FTΔ115 were measured to be 23, 13, and 7 min, respectively. Again, higher t_d values were found for longer mutant proteins.

The thermal unfolding of FTΔ45, FTΔ80, and FTΔ115 was monitored by recording the CD signals at 222 nm over a temperature range of 20−90 °C, using a heating rate of 1.0 °C/min. The results are shown in Figure 8. The thermal unfolding curves of FTΔ45 and FTΔ115 fit well to the equations established by Pace et al. (*29*). The analysis of FTΔ45 gave an onset of denaturation (T_d) of 50.2 °C, whereas that of FTΔ115 generated a T_d value of 60.0 °C. In contrast, the analysis of the thermal unfolding of FTΔ80 suggested a dissimilar process (*29*) in which the thermal unfolding was characterized by a T_{d1} value of 44.3 °C and a T_{d2} value of 72.0 °C. Consistent results were obtained by examining unfolding at different concentrations (0.03−0.3

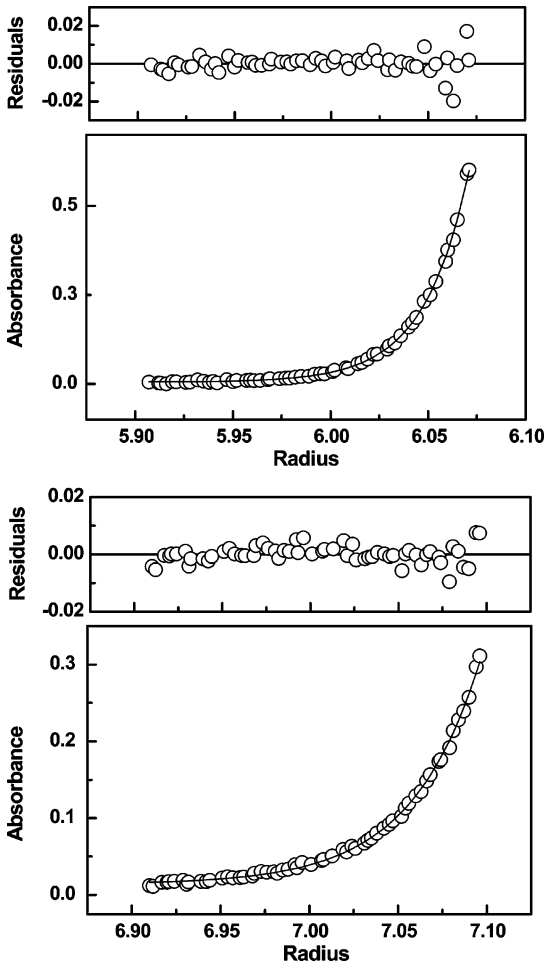

FIGURE 6: Equilibrium sedimentation of FTΔ45 and FTΔ115. (A) Equilibrium sedimentation of FTΔ45 (0.3 mg/mL) in 50 mM Tris buffer (pH 8.0) at 4 °C. (B) Equilibrium sedimentation of FTΔ115 under the same conditions. The absorbance at 280 nm is plotted against the radial position expressed in cm. The upper part of the figure shows the residual difference between experimental and fitted values by standard deviation. The average molecular masses of FTΔ45 and FTΔ115, calculated in terms of a single homogeneous species, were 115 671 and 45 697 Da, respectively.

mg/mL), the results of which indicated that the T_d values are concentration independent, but the extent of protein aggregation is reduced at lower concentration, as indicated by the optical density change of protein aggregates (data not shown). Coincidentally, the initial stage of FTΔ115, the final stage of FTΔ45, and the intermediate stage of FTΔ80 all had similar dichroic intensities. FTΔ80 likely acted in a way between FTΔ45 and FTΔ115 so that the data of FTΔ80 was divided into two parts. The T_{d1} value of FTΔ80 is lower than that of FTΔ45, and the T_{d2} value of FTΔ80 is higher than that of FTΔ115. The result reveals that FTΔ80 behaves like FTΔ45 at lower temperatures, whereas FTΔ80 acts like FTΔ115 at higher temperatures.

In the meantime, we also evaluated the thermal unfoldingof FTΔ28 and FTΔ66 (data not shown). The results of FTΔ28, FTΔ45, FTΔ66, and the first transition of FTΔ80 all followed the trend indicating that larger proteins have higher T_d values. On the basis of the CD measurements at 222 nm, FTΔ28 and FTΔ45 were stable, and their structures still remained ordered even when the temperature was raised above 60 °C. No aggregation was observed for FTΔ28 and FTΔ45 over the entire temperature range. However, the

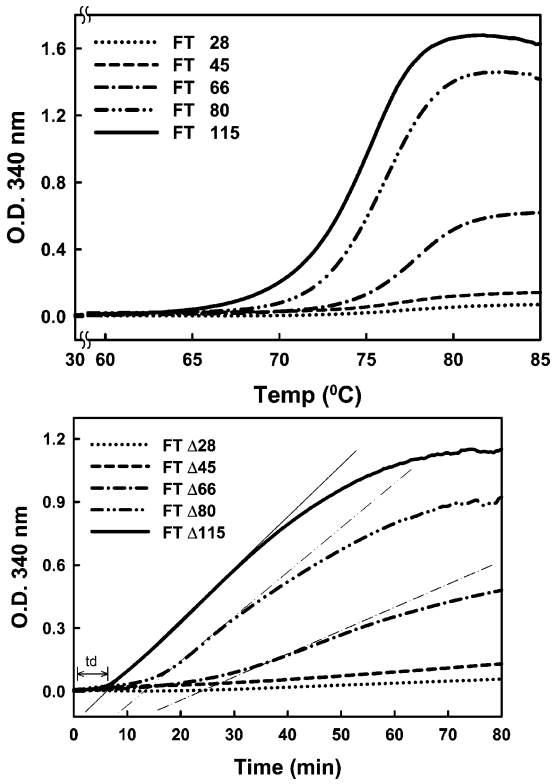

FIGURE 7: Thermal stability of various truncated FTs monitored by the optical density of protein aggregates. (A) Truncated FTs of 0.3 mg/mL were heat treated to evaluate temperature dependent denaturation and aggregation in 50 mM Tris buffer (pH 8.0). The optical density due to light scattering was measured at 340 nm with a heating rate of 1 °C/min. (B) Time dependent studies were carried out at 55 °C at the same wavelength.

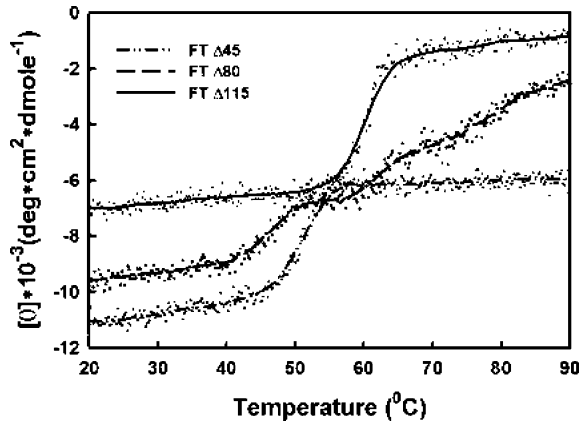

FIGURE 8: Thermal unfolding of FTΔ45, FTΔ80, and FTΔ115 monitored by CD spectroscopy at 222 nm. The CD melting curves were generated by monitoring the changes in the dichroic intensity at 222 nm as a function of temperature. The protein concentrations were 0.03−0.30 mg/mL in 50 mM Tris buffer (pH 8.0). Thermal denaturation was measured from 25 to 90 °C with a 1 °C interval increment.

denaturation process was irreversible, and no activity of FTΔ28 and FTΔ45 was found after thermal unfolding. Furthermore, the thermal unfolding of FTΔ115 directly resulted in the structural collapse and formation of protein aggregates. This phenomenon was similar to what was seen for FTΔ80 at the second transition (>70 °C), after which FTΔ80 precipitates were observed.

Because these proteins primarily differ by the number of heptad repeats, the repeats apparently help to maintain the

protein structure, which is consistent with the proposal that they form a leucine zipper (*19*). The fact that FTΔ80 forms precipitates and acts like FTΔ115 at higher temperature indicates that five heptads seem to be the minimum requirement. More repeats are thus required to maintain higher stability. In addition, the preliminary results evaluating the thermal inactivation suggested that FTΔ115 became completely inactive at 55 °C and that FTΔ45 required incubation at a higher temperature to be rendered inactive (data not shown). These detailed thermal inactivation studies are currently in progress and will be reported upon completion.

DISCUSSION

The α1,3-FT-catalyzed reaction proceeds with the inversion of configuration at the anomeric center of fucose. On the basis of the observation of a secondary isotope effect and the inhibition of GDP-2F-fucose, Wong and co-workers proposed the mechanism for human α1,3-FT V. Significant glycosidic bond cleavage occurs prior to the nucleophilic attack on the anomeric position of GDP-fucose (*23*). It is of interest to examine whether the *H. pylori* enzyme exerts a similar isotope effect and inhibition.

It has been reported that the 1,3/4-FTs of various *H. pylori* strains have 2−10 heptad repeats. For example, the *H. pylori* strain 11637 FT has 7 repeats, whereas strain 26695 has one FT with 2 repeats and one FT with 10 repeats (*17*, *19*, *30*). We conducted a systematic investigation of the effects of *C*-terminal truncation on the structure and function of *H. pylori* α1,3-FT. The resulting FTs that contain different length of heptad repeats are not only close to these FTs found in various *H. pylori* strains, but also useful for further comparative studies. Our results establish clear evidence supporting the idea that the tandem repeats are essential for forming a dimeric structure as well as structural stability. At least five repeats can be removed without affecting the FT activity because no obvious change was observed in the K_m and V_{max} values of FTΔ45, FTΔ66, and FTΔ80. Thus, the *C*-terminal 115 residues do not directly participate in the reaction mechanism. Because the analysis demonstrates that full enzyme activity is correlated with correct secondary and quaternary structure, truncated proteins FTΔ28, FTΔ45, FTΔ66, and FTΔ80 should have functions that are equivalent to the full-length enzyme. With the loss of the entire leucine zipper region, FTΔ115 has 20% of the original activity (based on V_{max} values) and becomes less stable at higher temperatures.

Ma et al. reported that residues 347−353 are involved in the determination of the 1,3- or 1,4-selectivity of the acceptor substrate (*24*, *31*). Thus, this region is likely a part of the acceptor-binding domain. Because it is also close to the heptad repeats that start at Asp364, the truncation of all of the repeats may exert more impact on the acceptor-binding site than on the donor site. This suggestion is clearly supported by the ∼13-fold increase in the K_m value of LacNAc in comparison with the ∼2.5-fold increase in the K_m value of GDP-fucose (when comparing FTΔ45 and FTΔ115). The result is also consistent with the fact that the two conserved motifs of α1,3/4-FT (sequences 164−182 and 231−263) known to participate in the binding of GDP-fucose are located relatively close to the *N*-terminus (*32*, *33*).

Most mammalian glycosyltransferases form a dimeric structure through disulfide bond formation, which has been found to be important for their secretion and localization (*34*−*36*). Dimerization, however, is not related to catalytic activity (*37*). Our results indicated that this *H. pylori* enzyme, in contrast, employs the tandem repeats for dimerization. The number of repeats is critical for dimeric structure formation. With less than five heptad repeats, the enzyme tends to be monomeric and less active. It will be intriguing to examine how a FT with a small (≤5) repeat number functions in vivo as well as address the issue of whether the resulting activity is correlated with the expression of Lewis antigens in *H. pylori*.

Moreover, FTs from various *H. pylori* strains have different levels of activity with varied acceptor specificities. The relative activities of α1,3/4-FT and α1,2-FT in a particular strain determine the expression pattern of Lewis antigens. The on/off status, relative expression levels, and the substrate specificity of different FTs are referred to as phase variation. Two common sequence features found in the gene for *H. pylori* α1,3/4-FT include a polyA-polyC tract in the 5′-end and a 21-mer repeat region (corresponding to the heptad repeats studied in this article) in the 3′-end (*17*, *38*). The length of polynucleotide repeats at the 5′-end determines the on/off switch by a strand slip mechanism, that is, replication errors due to slipped-strand base pairing in the repeat region (*39*). In *H. pylori*, there are two homologous α1,3/4-FT genes (*futA* and *futB*) and one gene (*futC*) that encodes α1,2-FT (*17*). The major difference between the *futA* and *futB* gene products is the number of leucine zipper-like repeats. Appelmelk et al. proposed that the *futA* gene product is responsible for the internal fucosylation of polymeric LacNAc, whereas the *futB* gene product preferentially fucosylates the terminal LacNAc (*39*). Nevertheless, a number of issues are still ambiguous and are not resolved by this hypothesis. For instance, the LPS of *H. pylori* contain multimeric fucose-containing Lewis antigens. Is it possible that the length of the heptad repeats is linked to the regulation of 1,3/4-FT activity? How do only the two enzymes (FutA and FutB) perform multiple α1,3/4-fucosylations? It will be of interest to study whether the tandem repeat length is involved in positioning fucosylation. The results presented here provide a good basis to tackle these unsolved questions. In summary, we report the first structural analysis of FT, concluding that the sequence 399−433, corresponding to the first five heptad repeats, is essential to the activity, as well as the integrity and stability of the secondary and quaternary structures.

ACKNOWLEDGMENT

We thank Dr. Hui-Chuan Chang for her considerable help in the biophysics studies, Dr. Chung-Yi Wu for his effort to prepare Gal*β*(1,4)GlcNAc-triazole, and Professor Gu-Gang Chang at the National Yang-Ming University for his critical reading of this manuscript and useful discussions.

REFERENCES

1. Dubois, A. (1995) Spiral bacteria in the human stomach: the gastric helicobacters, *Emerging Infect. Dis. 1*, 79−85.
2. Peterson, W. I. (1991) *Helicobacter pylori* and peptic ulcer disease, *N. Engl. J. Med. 324*, 1043−1048.
3. Parsonnet, J. (1996) *Helicobacter pylori* in the stomach—a paradox unmasked, *N. Engl. J. Med. 335*, 278−280.
4. Nakamura, S., Yao, T., Aoyagi, K., Iida, M., Fujishima, M., and Tsuneyoshi, M. (1997) *Helicobacter pylori* and primary gastric

lymphoma. A histopathologic and immunohistochemical analysis of 237 patients, *Cancer 79*, 3−11.
5. Ilver, D., Arnqvist, A., Ogren, J., Frick, I. M., Kersulyte, D., Incecik, E. T., Berg, D. E., Covacci, A., Engstrand, L., and Boren, T. (1998) *Helicobacter pylori* adhesin binding fucosylated histoblood group antigens revealed by retagging, *Science 279*, 373−377.
6. Guruge, J. L., Falk, P. G., Lorenz, R. G., Dans, M., Wirth, H. P., Blaser, M. J., Berg, D. E., and Gordon, J. I. (1998) Epithelial attachment alters the outcome of *Helicobacter pylori* infection, *Proc. Natl. Acad. Sci. U.S.A. 95*, 3925−3930.
7. Mahdavi, J., Sonden, B., Hurtig, M., Olfat, F. O., Forsberg, L., Roche, N., Angstrom, J., Larsson, T., Teneberg, S., Karlsson, K. A., Altraja, S., Wadstrom, T., Kersulyte, D., Berg, D. E., Dubois, A., Petersson, C., Magnusson, K. E., Norberg, T., Lindh, F., Lundskog, B. B., Arnqvist, A., Hammarstrom, L., and Boren, T. (2002) *Helicobacter pylori* SabA adhesin in persistent infection and chronic inflammation, *Science 297*, 573−578.
8. Linden, S., Boren, T., Dubois, A., and Carlstedt, I. (2004) Rhesus monkey gastric mucins: oligomeric structure, glycoforms and *Helicobacter pylori* binding, *Biochem. J. 379*, 765−775.
9. Kannagi, R., Izawa, M., Koike, T., Miyazaki, K., and Kimura, N. (2004) Carbohydrate-mediated cell adhesion in cancer metastasis and angiogenesis, *Cancer Sci. 95*, 377−384.
10. Dube, D. H., and Bertozzi, C. R. (2005) Glycans in cancer and inflammation−potential for therapeutics and diagnostics, *Nat. Rev. Drug Discovery 4*, 477−488.
11. Hynes, S. O., Keenan, J. I., Ferris, J. A., Annuk, H., and Moran, A. P. (2005) Lewis epitopes on outer membrane vesicles of relevance to *Helicobacter pylori* pathogenesis, *Helicobacter 10*, 146−156.
12. Moran, A. P., Prendergast, M. M., and Appelmelk, B. J. (1996) Molecular mimicry of host structures by bacterial lipopolysaccharides and its contribution to disease, *FEMS Immunol. Med. Microbiol. 161*, 105−115.
13. Lozniewski, A., Haristoy, X., Rasko, D. A., Hatier, R., Plénat, F., Taylor, D. E., and Angioi-Duprez, K. (2003) Influence of Lewis antigen expression by *Helicobacter pylori* on bacterial internalization by gastric epithelial cells, *Infect. Immun. 71*, 2902−2906.
14. Teixeira, A., David, L., Reis, C. A., Costa, J., and Sobrinho-Simoes, M. (2002) Expression of mucins (MUC1, MUC2, MUC5AC, and MUC6) and type 1 Lewis antigens in cases with and without *Helicobacter pylori* colonization in metaplastic glands of the human stomach, *J. Pathol. 197*, 37−43.
15. Backstrom, A., Lundberg, C., Kersulyte, D., Berg, D. E., Boren, T., and Arnqvist, A. (2004) Metastability of *Helicobacter pylori* bab adhesin genes and dynamics in Lewis b antigen binding, *Proc. Natl. Acad. Sci. U.S.A. 101*, 16923−16928.
16. Moran, A. P., Knirel, Y. A., Senchenkova, S. N., Widmalm, G., Hynes, S. O., and Jansson, P. E. (2002) Phenotypic variation in molecular mimicry between *Helicobacter pylori* lipopolysaccharides and human gastric epithelial cell surface glycoforms. Acid-induced phase variation in Lewis(x) and Lewis(y) expression by H. Pylori lipopolysaccharides, *J. Biol. Chem. 277*, 5785−5795.
17. Wang, G., Ge, Z., Rasko, D. A., and Taylor, D. E. (2000) Lewis antigens in *Helicobacter pylori*: biosynthesis and phase variation, *Mol. Microbiol. 36*, 1187−1196.
18. Kleene, R., and Berger, E. G. (1993) The molecular and cell biology of glycosyltransferases, *Biochim. Biophys. Acta 1154*, 283−325.
19. Ge, Z., Chan, N. W., Palcic, M. M., and Taylor, D. E. (1997) Cloning and heterologous expression of an alpha1,3-fucosyltransferase gene from the gastric pathogen *Helicobacter pylori*, *J. Biol. Chem. 272*, 21357−21363.
20. Wakarchuk, W. W., Cunningham, A., Watson, D. C., and Young, N. M. (1998) Role of paired basic residues in the expression of active recombinant galactosyltransferases from the bacterial pathogen *Neisseria meningitidis*, *Protein Eng. 11*, 295−302.
21. Lin, S. W., Wu, I. L., and Lin, C. H. (2005) Substrate specificity study of α1,3-fucosyltransferase from *Helicobacter pylori*. *Glycoconjugate J. 22*, 186. The preliminary result was also reported at the Glyco XVIII International Symposium on Glycoconjugates in September 4−9, 2005 in Florence, Italy.
22. Sambrook, J., Fritsch, E. F., and Maniatis, T. (1989) Molecular Cloning- A Laboratory Manual, 2nd ed, Cold Spring Harbor Laboratory, Cold Spring Harbor, NY.
23. Murray, B. W., Wittmann, V., Burkart, M. D., Hung, S. C., and Wong, C. H. (1997) Mechanism of human α1,3-fucosyltransferase V: Glycosidic cleavage occurs prior to nucleophilic attack, *Biochemistry 36*, 823−831.
24. Ma, B., Wang, G., Palcic, M. M., Hazes, B., and Taylor, D. E. (2003) *C*-terminal amino acids of *Helicobacter pylori* alpha1,3/4 fucosyltransferases determine type I and type II transfer, *J. Biol. Chem. 278*, 21893−21900.
25. Martin, S. L., Edbrooke, M. R., Hodgman, T. C., van den Eijnden, D. H., and Bird, M. I. (1997) Lewis X biosynthesis in *Helicobacter pylori*: Molecular cloning of an (1,3)-fucosyltransferase gene, *J. Biol. Chem. 272*, 21349−21356.
26. Sreerama, N., and Woody, R. W. (2004) Computation and analysis of protein circular dichroism spectra, *Methods Enzymol. 383*, 318−351.
27. Sreerama, N., and Woody, R. W. (2000) Estimation of protein secondary structure from circular dichroism spectra: comparison of CONTIN, SELCON, and CDSSTR methods with an expanded reference set, *Anal. Biochem. 287*, 252−260.
28. Sreerama, N., Venyaminov, S. Y., and Woody, R. W. (2000) Estimation of protein secondary structure from circular dichroism spectra: inclusion of denatured proteins with native proteins in the analysis, *Anal. Biochem. 287*, 243−251.
29. Pace, C. N. (1986) Determination and analysis of urea and guanidine hydrochloride denaturation curves, *Methods Enzymol. 131*, 266−280.
30. Rasko, D. A., Wang, G., Palcic, M. M., and Taylor, D. E. (2000) Cloning and characterization of the alpha(1,3/4) fucosyltransferase of *Helicobacter pylori*, *J. Biol. Chem. 275*, 4988−4994.
31. Ma, B., Lau, L. H., Palcic, M. M., Hazes, B., and Taylor, D. E. (2005) A single aromatic amino acid at the carboxyl terminus of *Helicobacter pylori* alpha-1,3/4 fucosyltransferase determines substrate specificity, *J. Biol. Chem. 280*, 36848−36856.
32. de Vries, T., Knegtel, R. M., Holmes, E. H., and Macher, B. A. (2001) Fucosyltransferases: structure/function studies, *Glycobiology 11*, 119R−128R.
33. Oriol, R., Mollicone, R., Cailleau, A., Balanzino, L., and Breton, C. (1999) Divergent evolution of fucosyltransferase genes from vertebrates, invertebrates, and bacteria, *Glycobiology 9*, 323−34.
34. Opat, A. S., Houghton, F., and Gleeson, P. A. (2000) Medial Golgi but not late Golgi glycosyltransferases exist as high molecular weight complexes. Role of luminal domain in complex formation and localization, *J. Biol. Chem. 275*, 11836−11845.
35. Fenteany, F. H., and Colley, K. J. (2005) Multiple signals are required for alpha2,6-sialyltransferase (ST6Gal I) oligomerization and Golgi localization, *J. Biol. Chem. 280*, 5423−5429.
36. El-Battari, A., Prorok, M., Angata, K., Mathieu, S., Zerfaoui, M., Ong, E., Suzuki, M., Lombardo, D., and Fukuda, M. (2003) Different glycosyltransferases are differentially processed for secretion, dimerization, and autoglycosylation, *Glycobiology 13*, 941−953.
37. Qian, R., Chen, C., and Colley, K. J. (2001) Location and mechanism of alpha 2,6-sialyltransferase dimer formation. Role of cysteine residues in enzyme dimerization, localization, activity, and processing, *J. Biol. Chem. 276*, 28641−28649.
38. Appelmelk, B. J., Shiberu, B., Trinks, C., Tapsi, N., Zheng, P. Y., Verboom, T., Maaskant, J., Hokke, C. H., Schiphorst, W. E., Blanchard, D., Simoons-Smit, I. M, van den Eijnden, D. H., and Vandenbroucke-Grauls, C. M. (1998) Phase variation in *Helicobacter pylori* lipopolysaccharide, *Infect. Immun. 66*, 70−76.
39. Appelmelk, B. J., Martin, S. L., Monteiro, M. A., Clayton, C. A., McColm, A. A., Zheng, P., Verboom, T., Maaskant, J. J., van den Eijnden, D. H., Hokke, C. H., Perry, M. B., Vandenbroucke-Grauls, C. M., and Kusters, J. G. (1999) Phase variation in *Helicobacter pylori* lipopolysaccharide due to changes in the lengths of poly(C) tracts in alpha3-fucosyltransferase genes, *Infect. Immun. 67*, 5361−5366.

BI0601297